Bioorganic & Medicinal Chemistry 25 (2017) 5875–5888

Contents lists available at ScienceDirect

Bioorganic & Medicinal Chemistry

journal homepage: www.elsevier.com/locate/bmc

The compound (3-{5-[(2,5-dimethoxyphenyl)amino]-1,3,4-thiadiazolidin-2-yl}-5,8-methoxy-2*H*-chromen-2-one) inhibits the prion protein conversion from PrP^C to PrP^{Sc} with lower IC_{50} in ScN2a cells

Nataraj S. Pagadala [a,*], Trent C. Bjorndahl [b], Michael Joyce [a], David S. Wishart [b], Khajamohiddin Syed [c], Abdolamir Landi [a,d]

[a] Department of Medical Microbiology and Immunology, 6-020 Katz Group Centre, University of Alberta, Edmonton, Alberta T6G 2E1, Canada
[b] Department of Biological Sciences, and Computing Science, University of Alberta, Edmonton, Alberta T6G 2E8, Canada
[c] Unit for Drug Discovery Research, Department of Health Sciences, Faculty of Health and Environmental Sciences, Central University of Technology, Bloemfontein 9300, Free State, South Africa
[d] Department of Immunology, School of Medicine, Ahvaz Jundishapur University of Medical Sciences, Ahvaz, Iran

ARTICLE INFO

Article history:
Received 28 June 2017
Revised 16 September 2017
Accepted 18 September 2017
Available online 19 September 2017

Keywords:
Prion
Docking
HQSAR
CoMFA
NMR
ScN2a cells

ABSTRACT

Prion diseases are fatal neurodegenerative disorders of the central nervous system characterized by the accumulation of a protease resistant form (PrP^{Sc}) of the cellular prion protein (PrP^C) in the brain. Two types of cellular prion (PrP^C) compounds have been identified that appear to affect prion conversion are known as Effective Binders (EBs) and Accelerators (ACCs). Effective binders shift the balance in favour of PrP^C, whereas Accelerators favour the formation of PrP^{Sc}. Molecular docking indicates EBs and ACCs both bind to pocket-D of the $SHaPrP^C$ molecule. However, EBs and ACCs may have opposing effects on the stability of the salt bridge between Arg^{156} and Glu^{196}/Glu^{200}. Computational docking data indicate that the hydrophobic benzamide group of the EB, GFP23 and the 1-(3,3-dimethylcyclohexylidene)piperidinium group of the ACC, GFP22 play an important role in inhibition and conversion from $SHaPrP^C$ to $SHaPrP^{Sc}$, respectively. Experimentally, NMR confirmed the amide chemical shift perturbations observed upon the binding of GFP23 to pocket-D of $SHaPrP^C$. Consistent with its role as an ACC, titration of GFP22 resulted in widespread chemical shift changes and signal intensity loss due to protein unfolding. Virtual screening of a ligand database using the molecular scaffold developed from the set of EBs identified six of our compounds (previously studied using fluorescence quenching) as being among the top 100 best binders. Among them, compounds 5 and 6 were found to be particularly potent in decreasing the accumulation $SHaPrP^{Sc}$ in ScN2a cells with an IC_{50} of ~35 μM and 20 μM.

1. Introduction

Prion diseases or transmissible spongiform encephalopathy's (TSEs) that include Creutzfeldt-Jakob disease (CJD), chronic wasting disease (CWD), scrapie, and bovine spongiform encephalopathy (BSE) are neurodegenerative diseases characterized by the accumulation of a protease resistant form of the prion protein (PrP^{Sc}) in the brain.[1,2] Currently, no effective therapy or vaccine exists on these invariably fatal TSEs. Studies have shown that disease associated forms of prion arises when the α-helical rich normal cellular prion protein (PrP^C) gets converted to a β- sheet rich disease-related isoform PrPSc.[3] The propensity of PrP misfolding is determined by the difference in electrostatic energies namely salt bridge and solvation energies between folded and misfolded states and the magnitude of energy barrier separating them.[4] The disruption of these electrostatic salt bridges in native PrP^C leads to the formation of more hydrophobic PrP^{Sc}. Structurally, these salt bridges are differentiated into local and non-local based on the participating residues and their proximity in sequence. Local salt bridges, like Asp^{148}-Glu^{152} in α1, Asp^{208}-Glu^{211} in α3, and Arg^{164}-Asp^{167} between β2 and the following loop, serve to stabilize secondary structural elements of the protein; nonlocal salt bridges, like Arg^{156}-Glu^{196}, Arg^{164}-Asp^{178}, and Glu^{146}-Lys^{204}, help to hold these elements together in the overall tertiary fold[4] . There is increasing interest in developing an antiprion compound to inhibit the conversion of PrP^C to PrP^{Sc} to provide control over TSE disease keeping the salt bridges intact. While the mechanisms of prion propagation are not well understood, numerous studies have

* Corresponding author at: Medical Microbiology and Immunology, Li Ka Shing Institute of Virology, University of Alberta, Edmonton, AB T6G 2E1, Canada.
E-mail address: nattu251@gmail.com (N.S. Pagadala).

https://doi.org/10.1016/j.bmc.2017.09.024
0968-0896/

endeavored to develop the therapeutics that prevent the conversion of PrP^{C} to PrP^{Sc} thus preventing neurodegeneration.[5] Experimental studies of various compounds (polyanionic agents, Congo red, amphotericin B, porphyrins, and phenothiazine derivatives, such as quinacrine) have had antiprion effects, reducing PrP^{Sc} accumulation in cell culture models of prion diseases.[6] In comparison to the known compounds, an antiprion compound known as GN8 was shown to be more effective than quinacrine in preventing the accumulation of PrPSc.[7] Nuclear Magnetic Resonance (NMR) studies on the chemical shift changes caused by GN8 binding show that the major binding region is located in the C-terminal domain of PrPC.[8] Furthermore, 2-aminothiazoles that improved metabolic stability and membrane permeability in mice represents a promising new class of drug leads for treating prion diseases. Some of these compounds potently inhibit the conversion of PrP^{C} to PrPSc.[9] Later, a variety of structurally diverse compounds were identified as potent inhibitors or accelerators of PrP^{C}. These compounds were classified into effective binders (EBs), effective low affinity binders (ELBs), non-effective binders (NEBs), non-effective low affinity binders (NELBs), or accelerators (ACCs).[10] Recently, the analog of indole, IND22308 produced a large effect in HTS and SPC assays with 70% and 94% inhibition. In addition, the compound showed no effect on cell viability in both stationary phase and in dividing cells elucidating the antiprion activity with an EC50 of 7.5 and 1.6 μM.[11] Although various strategies for drug discovery of antiprion compounds have been reported, there have been no reports on the binding regions of antiprion compounds that include evidence for interaction with specific amino acid residues. To design more potent and highly specific antiprion compounds for TSE disease, molecular recognition of compounds by the prion protein has to be clearly understood. In this study, to elucidate the mechanism of PrP^{C} stabilization or conversion to PrP^{Sc}, and to understand the individual atomic contributions that play an important role in the antiprion activity, the binding of a series of the known compounds, EBs and ACCs to $SHaPrP^{C}$ were examined using molecular docking. The nomenclature of the compounds was exactly represented the same in the published paper for better understanding.[10] In addition, NMR studies were conducted for two representative known compounds, GFP23 (EB, $C_{19}H_{30}N_5$) and GFP22 (ACC, $C_{21}H_{24}N_2O_2$) to examine their effect in stabilizing or misfolding of $SHaPrP^{C}$. Further, 3D QSAR models were built for these known compounds EBs and ACCs using HQSAR (Hologram quantitative structure activity relationship, Tripos Inc) and CoMFA (comparative molecular field analysis) to understand the individual atomic contributions that play an important role in the biological activity and intermolecular interactions against SHaPrPC.[12] To facilitate further development of new antiprion compounds, a molecular scaffold was generated by the set of known compounds EBs. Virtual screening of the compound database using newly generated scaffold identified a total of 100 compounds with 85% similarity. Out of these 100 compounds, six compounds (Bionet1G037 ((5-(3,4-dimethoxyphenyl)-4-methylpyrimidin-2-amine) ($C_{13}H_{15}N_3O_2$)), Bionet5T0214 ((4,5-bis(4-methoxyphenyl)pyrimidin-2-amine ($C_{18}H_{17}N_3O_2$)), Bionet6T0265 ((4,5-bis(4-methoxyphenyl)-1,3-thiazol-2-amine ($C_{17}H_{16}N_2O_2S$)), chembridge6413213 ((*N*-[4-(2,5-Dimethoxyphenyl)-5-methyl-1,3-thiazol-2-yl]-3,4,5-trimethoxybenzamide) ($C_{22}H_{24}N_2O_6S$)), Chembridge6623338 ((3-{5-[(2,5-dimethoxyphenyl)amino]-1,3,4-thiadiazol-2-yl}-8-methoxy-2*H*-chromen-2-one) ($C_{20}H_{17}N_3O_5S$)), and chembridge6872366 ((4-(2,4-dimethoxyphenyl)-5-methyl-1,3-thiazol-2-amine) ($C_{12}H_{14}N_2O_2S$)) had been used previously for fluorescence quenching studies against SHaPrPC.[13] These six representative compounds were further investigated experimentally in prion infected ScN2a cells. They show antiprion activity in reducing the accumulation of PrP^{Sc} in a high-throughput assay using scrapie-infected neuroblastoma ScN2a cell lines at a minimum concentration of 20 μM. All of these six representative antiprion compounds were non-toxic to ScN2a cell culture. Taken together, the results suggest that the antiprion activity of these six compounds is mainly mediated by binding to pocket-D of $SHaPrP^{C}$. Further, the intact salt bridge between Arg^{156}/Glu^{196}/Glu^{200} may play an additional role in the prevention of formation of $SHaPrP^{Sc}$.

2. Results and discussion

2.1. Effective binders (inhibitors) stabilize pocket-D through hydrogen bonding network

To examine the mode of binding of EBs, we performed blind docking with a set of compounds known as EBs against $SHaPrP^{C}$ using the dock module of MOE software suite 2014.[10] Docking studies indicated that these ligands to bind in a hydrophobic pocket-D where the known compounds 2-aminothiazoles bound. The benzamide group of EB (**GFP23**, $C_{19}H_{30}N_5$) orients towards the binding pocket while the 1H indole group is solvent exposed with the interaction energy of −12.6 kcal/mol (Fig. 1).

In the docked complex, EB (GFP23, $C_{19}H_{30}N_5$) made two hydrogen bonds with Asn197 (N) and Asp202 (Oδ1) and makes hydrophobic contacts with Arg^{156} (N), Asn^{197} (N), Phe^{198} (Cβ) and Met^{206} (C) along with one water molecule in the vicinity of the binding pocket. The benzamide oxygen interacts with the nitrogen atom of Asn^{197} and also makes a hydrogen bond to Thr^{192} through water. In addition, the oxygen atom attached to 1H-indole group interacts with the positively charged residue Arg^{156} at 3.01 Å distance. The carbon atoms C5 and C9 of the benzamide made hydrophobic contacts with the residues Met^{206} and Phe^{198} at 3.55 and 3.23 Å distances, respectively. This predicted orientation of binding indicates that the presence of the benzamide group attached to 1H-indole plays an important role in inhibition $SHaPrP^{C}$ conversion. The experimental dissociation constant (K_d) was determined to be 51.2 ± 12.2 μM.[10] The compound2 (GFP06, $C_{20}H_{22}N_2O$) also has a good docking score with the interaction energy of −11.1 kcal/mol. Due to its bigger size, the tetrahydronaphthalen-2-yl acetamide group occupies more space in the binding site making a hydrogen bond with oxygen atom of Asn^{197} and two hydrophobic contacts with Phe^{198} (C2) and Met^{206} (C). The 1H-indole nitrogen on the pocket surface makes a water mediated interaction with Gly^{195} while the acetamide group accepts electrons from Tyr^{149} (Fig. S1A). The estimated K_d value was determined to be 48.6 ± 20.3 μM.[10] The tricyclic group of the compound3 (GPF04, $C_{18}H_{23}N_3O_2S$) made a hydrogen bond with

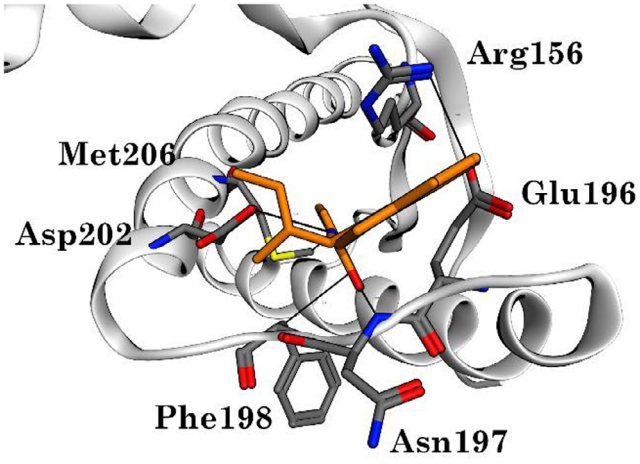

Fig. 1. Binding mode of the inhibitor (GFP23) in the binding pocket-D of $SHaPrP^{C}$.

Asn[153] and H—Pi interaction with Arg[156] on the surface of the pocket. The nitrogen atom of 2,3-pyrimidin-4 methyl accepts electrons from Tyr[149] while methyl cyclohexamine enters deeper into the pocket interacting with Phe[198] (Cβ), Ile[203] (C1) with the total interaction energy of −11.3 kcal/mol (Fig. S1B). The compounds 4 and 7 (GFP75, $C_{17}H_{15}N_3O_2S$) and (GJP45, $C_{18}H_{19}N_3O_S$) have the same affinity of −12.2 kcal/mol, without showing any hydrogen bonds with SHaPrP^C. The indole group of compound4 makes two hydrophobic contacts with Phe[198] and Met[206], but 2-(thieno[2,3-*d*]pyrimidin-4-methyl is exposed and makes a H—Pi interaction with Glu[196] (Fig. S1C and F). The nitrogen atom of 2,3-pyrimidin of compound4 makes a water-mediated interaction with the positively charged residue Arg[156]. The 3-amino-*N*-cyclopentylthieno group of the compound7 (GJP45, $C_{18}H_{19}N_3O_S$) penetrates deeply into the binding pocket and makes five hydrophobic contacts with Met[154], Phe[198], Ile[205], Met[206] and Val[209] (Fig. S1F). The amino-*N*-cyclopentylthieno also has a water-mediated and H—Pi interactions with Arg[156], Glu[196] and Asp[202]. The compounds 5 & 10 (GFP80, $C_{21}H_{21}N_3O_2$ & GJP52, $C_{23}H_{20}N_20$) also have equal affinity with the interaction energy of −12.1 kcal/mol. The di-hydroquinazolin ring of compound5 occupies the surface of the pocket and forms hydrogen bonds with Arg[156] and Asn[153] while the naphthalene ring occupies a hydrophobic patch, contacting Phe[198] (Cβ), of Ile[184] (C2), Ile[203] (C1) and Met[206] (Cβ) (Fig. S1D). This compound also makes water-mediated hydrogen bonds with Glu[196], Arg[156] and Gly[195] in the vicinity of the binding site. However, *N*-(pyridin-2-ylmethyl)acetamide group of compound10 orients towards the hydrophobic patch making a hydrogen bond with Asn[197] and hydrophobic contacts with Phe[198] (Cβ), Ile[203] (C1) and Met[206] (C). The tricyclic group makes H—Pi interaction with Arg[156] on the surface of the binding pocket (Fig. S1I). The tricyclic group (6-methyl-2,3,4,4a,9,9a-hexahydro-1*H*-carbazol-1-one) of compound6 (GJP14, $C_{21}H_{28}N_2O_2$) is placed above the surface of the binding pocket showing H—Pi interaction with Arg[156]. The piperidine group is oriented towards the hydrophobic patch of the pocket and forms hydrogen bonds and hydrophobic contacts with Asn[197], Asp[202], Phe[198] and Met[206]. The residue Arg[156] donates electrons to the hydroxyl group of the compound along with Asn[197], while Tyr[149] donates its electrons to the oxygen attached to the tricyclic group (Fig. S1E). The piperidine group also has an ionic interaction with negatively charged Asp[202] with the total interaction energy of −12.0 kcal/mol. This binding orientation showed that the piperidine group of compound6 is mainly responsible for the inhibition of prion pathogenic conversion from PrP^C–PrP^{Sc}. Previous experimental studies conducted on a total of 47 derivatives of compound6 revealed that, a tricyclic aromatic scaffold, a hydroxy group, and a terminal amino group were determined to be the basic requirements for antiprion activity.[14] NMR analysis also showed that this compound6 binds to same region of PrP^C that corresponds to that of GN8 which undergoes a global fluctuation in a time scale of micro- to milliseconds.[15] The compound8 (GJP49, $C_{19}H_{24}N_2O_2S$) had a higher binding affinity compared to other compounds, with the total binding energy of −14.1 kcal/mol (Fig. S1G). The methyl group on the C1 carbon atom of 2-piperidine makes three hydrophobic contacts with Phe[198], Met[206] and Ile[203], while the dioxino[2,3-*g*]quinolone group interacts with an OH group of Tyr[140] via a hydrogen bond. Since this compound does not have any water mediated-interactions in the vicinity of the binding site, the bulky group of 2,3-dihydro[1,4]-dioxino[2,3-*g*]quinolone attached to 7-{[2-(piperidin-1-yl)ethyl]-sulfanyl} is responsible for higher binding energy compared to other tricyclic groups of compounds 3 & 6. Finally, the compound 9 (GJP51, $C_{18}H_{20}N_2OS$) had lower binding energy compared to all the other EBs with the binding energy of −10.6 kcal/mol. The thiophen group is oriented towards the hydrophobic portion of the binding pocket making a H—Pi interaction with Tyr[157] (Fig. S1H). The (2*Z*)-2-(2,3,3-trimethyl-3,4-dihydroisoquinolin-1(2*H*)-ylidene)ethanamide is placed on the surface without any contacts with SHaPrP^C. These docking studies and previous experimental data confirms that all these EB's were commonly bind to major binding pocket-D of SHaPrP^C and may keep the salt bridge between Arg[156] and Glu[196] intact [10]. Overall, ligand protein interactions show that Asn[197], Phe[198], Thr[201], Asp[202], Ile[203], Ile[205] and Val[206] residues acts as common pharmacophores of all these EB's preventing the prion conversion to pathogenic form from SHaPrP^C to SHaPrP^{Sc} (Fig. 2).

2.2. Accelerators (ACCs) attenuates PrP flexibility

To predict the role of the residues in protein misfolding, second set of the molecules known as accelerators (ACCs) were docked with SHaPrPC.[10] The 1-{3-[2-(4,6-dimethylpyrimidin-2-yl)hydrazin-1-yl] group of compound1 (GFP22, $C_{21}H_{24}N_2O_2$) orients towards Tyr[149] on the surface of the pocket making a hydrogen bonded with the hydroxyl group of Tyr[149]. The nitrogen atom of hydrazine donates a proton to the hydroxyl group of Tyr[149] (Fig. 3).

The 5,5-dimethylcyclohex-3-en-1-ylidene}-15-piperidin-1-ylium ring orients towards Glu[196] without making any contacts with pocket-D of SHaPrP^C. This compound1 binds with a high interaction energy of −13.7 kcal/mol. The compounds 2, 3 and 4 bind with equal affinities, −11.1, −11.2 and −11.5 kcal/mol, respectively. The tricyclic group of the compound2 (GFP88, $C_{18}H_{20}N_4S$) *N*-(propan-2-yl)-2-(pyridin-3-yl)-4b,5,6,7,8,8a-hexahydro[1]benzothieno[2,3-*d*] oriented into the binding pocket while pyrimidin-4-amine was above the surface of the pocket making a H—Pi interaction with Arg[156]. The nitrogen atom of pyrimidin-4-amine also makes water-mediated interactions with Arg[148] and Asn[153] (Fig. S2A). However, the nitrogen atom of the tricyclic group interacts with the negatively charged Glu[196] while the cyclohexane ring of the tricyclic group shows contacts with Phe[198]. The cyclohexane ring of compound3 (GFP92, $C_{20}H_{27}N_3O_3$) occupies a deeper part of the binding pocket-D compared to tricyclic group while imidazolidine-2,4-dione resides very close to Tyr[149] and Arg[156] and makes two hydrogen bonds with Met[206] (C) and Tyr[149] (OH) and three hydrophobic contacts with Phe[198] (Cβ), Asn[153] (O1) and Asp[202] (O1). One of the oxygen atoms of imidazolidine-2,4-dione shows hydrogen bond with Tyr[149] while the other

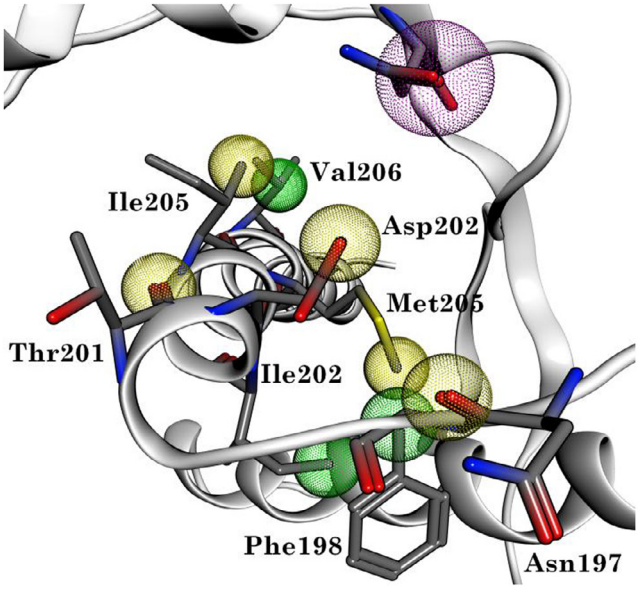

Fig. 2. Pharmacophores of the inhibitor (GFP23) in the binding pocket of SHaPrP^C.

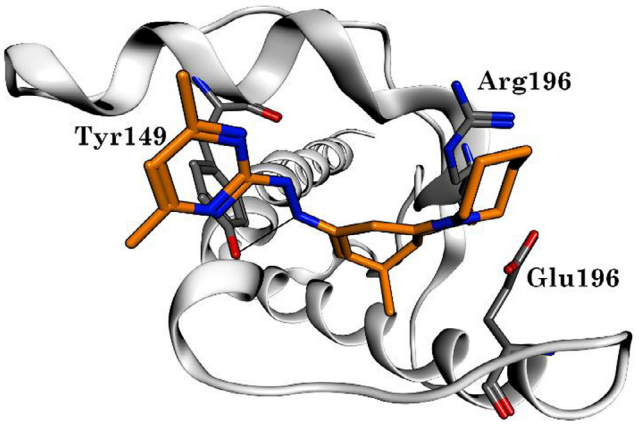

Fig. 3. Binding mode of the accelerator (GFP22) in the binding pocket-D of SHaPrP$^{C.}$

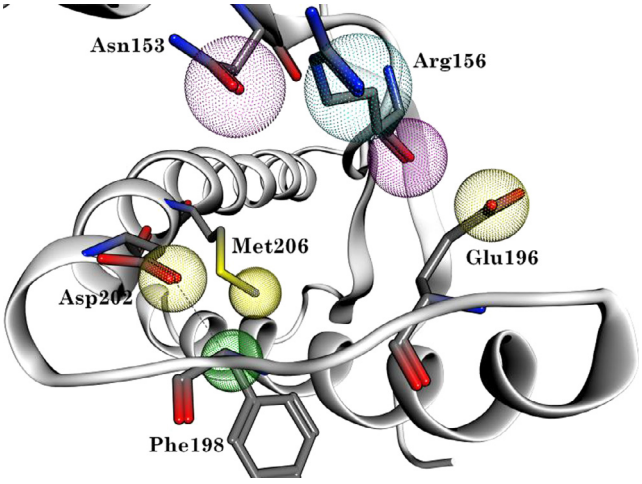

Fig. 4. Pharmacophores of the accelerator (GFP22) in the binding pocket of SHaPrP$^{C.}$

oxygen atom makes water-mediated contacts with Arg^{156} and Gly^{195} (Fig. S2B). The *N*-(2-phenylethyl)propanamide is placed above the surface of the pocket and shows no contacts with pocket-D. The data obtained for compound4 (GFP94, $C_{18}H_{19}ClN_2O_2$) indicate that the nitrogen atom of the *N*-(4-chloro-2-methoxy-5-methylphenyl) interacts with Asn^{153} through a hydrogen bond while chlorine has hydrophobic contacts with the backbone atoms of Phe^{198} and the side chain of Met^{206}. The 2,3-dihydro-1*H*-indol-1-yl group is on the surface and has no contacts with pocket-D while the acetamide group has water-mediated interactions with Gly^{195} and Glu^{196} (Fig. S2C). The total interaction energy with the protein is −10.2 kcal/mol. The molecular docking performed for compound5 (GFP39, $C_{22}H_{25}N_3O_3$) suggests that the terminal methybenzene and cyclohexyl rings occupy space on the surface of the protein because of a larger chain length between the two rings. The nitrogen atom of *N*-(cyclohexylmethyl)acetamide penetrates slightly deeper into the pocket making contacts with Tyr^{149} and Asp^{202} through hydrogen bonds while pyrolidine has a hydrophobic contact with Phe^{198}. The nitrogen atom also makes a water-mediated interaction with Arg^{156} (Fig. S2D). The final model obtained for compound6 (GJP41, $C_{18}H_{28}N_4OS$) showed that 4-propyl-1,2,4-triazolidin-3-yl}pyridine penetrates very deeply into the pocket while cyclohexane carbaldehyde is exposed to the surface. Compound6 makes three hydrogen bonding and hydrophobic interactions with Tyr^{149}, Asp^{202}, Asn^{153} and Phe^{198} and has a higher interaction energy, −12.4 kcal/mol compared to compounds 2, 3, 4 and 5, respectively (Fig. S2E). One of the nitrogen atoms of 1,2,4-triazolidin of compound6 accepts electrons from Arg^{156} while the other nitrogen donates electrons to oxygen atom of Asp^{202}. The nitrogen atom also donates protons to backbone of Asn^{153} that occupies between pro^{158} and Tyr^{157}. These results also show that all these ACCs bind to pocket-D and may disturb the salt bridge between Arg^{156}/Glu^{196}/Glu^{200} which might play an important role in prion conversion from SHaPrP^{C} to SHaPrP^{Sc}. Overall, ligand protein interactions show that Asn^{153}, Arg^{156}, Glu^{196}, Phe^{198} and Asp^{202} residues act as common pharmacophores of these compounds accelerating the prion conversion to pathogenic form from SHaPrP^{C} to SHaPrP^{Sc} (Fig. 4).

2.3. NMR studies of EB (GFP23) and ACC (GFP22)

The binding site for the EB (GFP23) and ACC (GFP22) was investigated using heteronuclear NMR spectroscopy on a 15N-labeled sample of the SHaPrP^{C} (amino acids 90–232 with C-terminal 6× -His tag). Titration of GFP22 resulted in widespread chemical shift changes and signal intensity loss due to protein aggregation (Fig. 5A). Fig. 5B showed the signal attenuation and chemical shift changes in the 15N-HSQC spectrum of the SHaPrP^{C} after addition of EB (GFP23) (5:1, ligand/protein molar ratio). The first set of attenuated signals (Y^{157}, G^{195}, and T^{199}) were located in pocket-D located between the helices α2, α3 and loop 4, which is considered a hotspot for inhibition of conversion of SHaPrP^{C} to SHaPrP^{Sc} with antiprion compounds.[16] The second set of attenuated signals were seen in an unstructured loop with the residues G^{123}, M^{129}, V^{166}, and Y^{169} adjacent to α1, which also contains two tyrosine's and a tryptophan residue (Fig. 5B).

In addition, a first region of the protein (pocket-D) undergoes conformation change, due to small changes in lengths of the hydrogen bond or other minor conformational/dynamic changes. However, no NOEs were observed between the inhibitor and the region in pocket-A, which consists of the 'amylome' residues ^{169}NNQNNY^{175}.[14] Long-range effects of this region and the distal residues in α3 have been noted in previous studies.[17] Whether these distal effects on the amylome region upon inhibitor binding have any significance or are an inconsequential artifact has yet to be determined.

2.4. HQSAR study of EBs and ACCs

Since there are a variety of differing structures in both the EB (GFP23) and ACC (GFP22) we wished to examine which areas of each molecule were important for binding to PrP^{C} and inhibiting PrP^{sc} formation. In an effort to create a scaffold on which to build new inhibitors of prion formation, we first performed a quantitative structure activity relationship using HQSAR in order to asses which portions of EBs and ACCs were important for their respective activity. The ability of each EB to inhibit the formation of PrP^{Sc} was obtained from previously published western blots results that examined the ability of compounds to block PrP^{Sc} formation. The EBs were then fragmented *in silico* and the composite data set used to examine which fragments correlated with biological activity. To obtain the best cross validated r^2 of the model, HQSAR analysis was performed with a set of factors such as fragment size, number of fragments, atom types (A), bond types (B), atom hybridization or connectivity (C), hydrogen bond and donor (H). The rules to determine the type of unique structural features of the model comps were provided by user-selectable flags including A, B, C and H. Atom flag differentiates the fragments based on different types of element. Different bond types of these fragments were distinguished using bond's flag. The hybridization state of the atoms in the fragment was distinguished using connection flag. Hydrogen

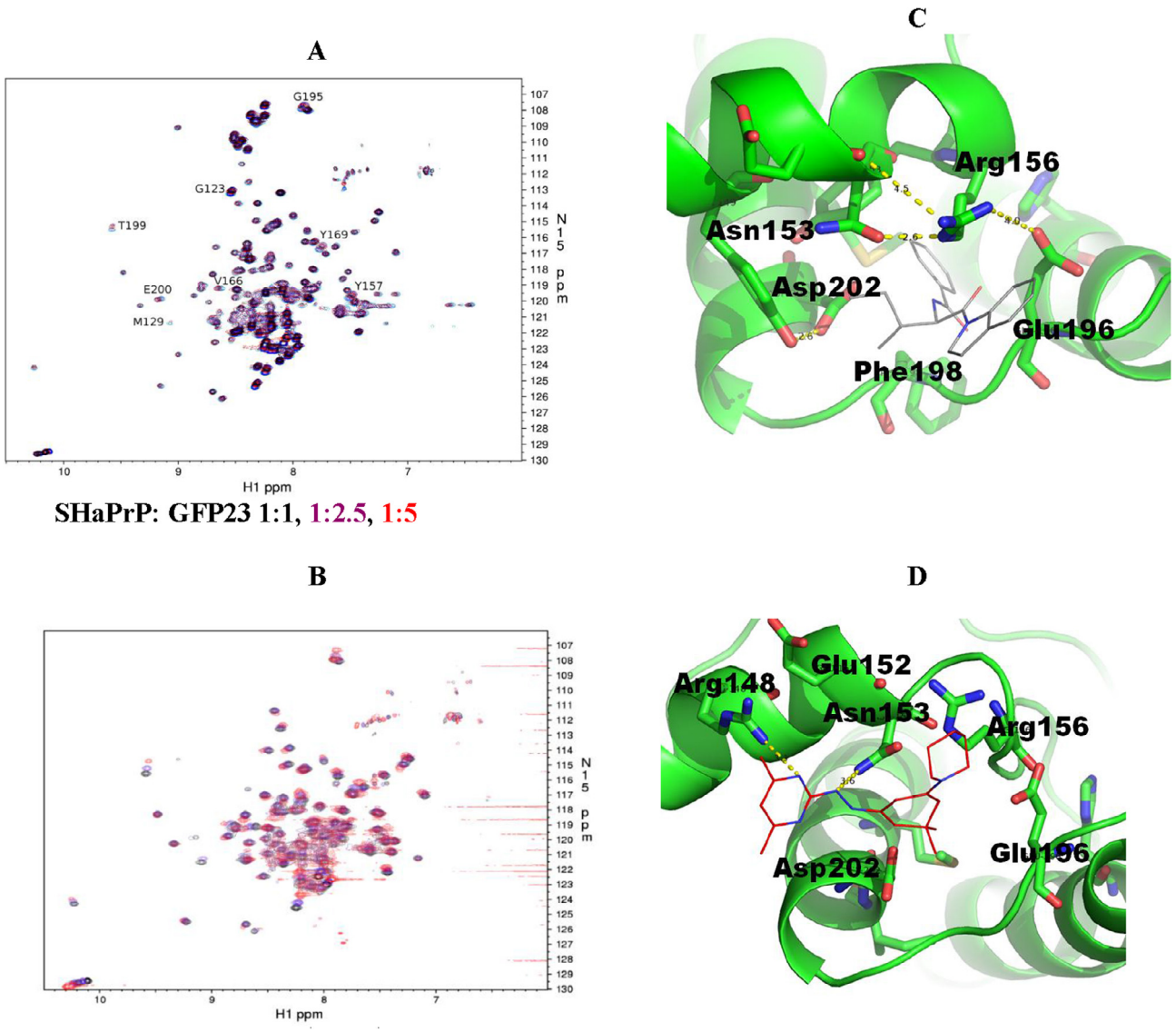

Fig. 5. ^{15}N-HSQC titration spectra of an inhibitor (GFP23) (Fig. A) and accelerator (GFP22) (Fig. B) of $SHaPrP^{C90-232}$ destabilization. General random coil shifts readily present at a 1:5 ratio of protein to ligand. The bound box was defined by the residues presenting the largest chemical shift changes observed upon ligand titration for the inhibitor, GFP23 (Fig. C) and the accelerator, GFP22 (Fig. D).

flag distinguishes whether or not hydrogen atoms are included in the fragment. In the initial HQSAR analysis, several combinations of these parameters were considered including the default fragment size of 4–7 atoms including atom types (A), bond types, (B), connectivity (C), and hydrogen (H). HQSAR analysis was performed over the 12-default series of hologram lengths of 53, 59, 61, 71, 83, 97, 151, 199, 257, 307, 353, and 401 bins. Next, the partial least squares (PLS) analysis that gave the least cross-validated standard error (SEcv) was selected for obtaining the best hologram length (L) and optimum number of components (N). Finally, an HQSAR model (hologram) was derived from the training set. The results obtained from HQSAR analyses for the 21 training set comps using several fragment distinction combinations are summarized in Table 1.

The best HQSAR model was generated (descriptors: atoms, bonds, hydrogen's, donors and acceptors; fragment length: 4.7, hologram length: 353). The PLS analysis for the training set yielded the best model (Table 3) with a cross-validated q^2 value of 0.230 with five optimal components, and non-cross validated r^2 value of 0.97 with a standard error of 0.077. The PLS analysis was repeated using the best fragment distinction obtained from previous step to check its influence on key statistical parameters. The statistical results of the different fragment sizes evaluated (2–5, 3–6, 5–8, 6–9, 7–10 and 8–11) are summarized in Table 2.

The results show that the best statistical result was obtained with the fragment size 4–7. The predictive ability of the best HQSAR model derived using the 21 training set molecules was validated by external test set of 4 compounds randomly picked (marked asterisk in Table 1), giving satisfactory predictive r^2 value of 0.73 (Table 3).

The experimental and predictive activities of both training set and test set were shown in Table 4. Based on the HQSAR model, the relationship between the experimental and predicted activities of both the training and test set were fairly predicted with r2 value of 0.73 and residual values less than one log unit (Fig. S3 and Table 4). In addition to predicting the activities of unknown molecules, the QSAR model also provides clues to the relation of different molecular fragments of biological activity.

Table 1
HQSAR analysis for various fragment distinctions of BE and BNE using fragment size (4–7).

Model No	Fragment Distinction	Statistical parameters				
		q^2	r^2	SEE	N	HL
1	A/B					
2	A/B/C	–	–	–	–	–
3	A/B/C/H	–	–			
4	A/B/C/Ch	0.050	0.869	0.081	3	307
5	A/B/C/H/Ch	0.230	0.970	0.077	5	353
6	A/C/DA	–				
7	A/B/C/H/DA	0.104	0.983	0.084	5	353
8	A/B/H	0.235	0.983	0.077	5	199
9	A/B/H/DA	0.127	0.781	0.077	3	353
10	A/B/C/DA					
11	**A/B/Ch/DA**					
12	A/B/H/Ch	0.072	0.566	0.078	2	151
13	A/B/DA					
14	A/B/Ch					
15	A/C/Ch/DA					
16	**A/C/H/DA**	**0.511**	**0.994**	**0.064**	**6**	**97**

q2 Cross-validated correlation coefficient, r2 non-cross-validated correlation coefficient, SEE standard error of estimate, N number of statistical components, HL hologram length, A atoms, B bonds, C connection, H hydrogen atoms, Ch chirality, DA donor and acceptor
[a]The model chosen for HQSAR analysis.

Table 2
Influence of various fragment sizes using the best fragment distinction combination (A/C/Ch/DA) using HQSAR analysis.

Model No	Fragment Size	Statistical parameters				
		q^2	r^2	SEE	N	HL
1	2–5	–				
2	3–6					
4	5–8	0.067	0.809	0.080	3	97
5	6–9	–	–	–		–
6	7–10	–	–	–	–	–
7	8–11	–	–	–		

Table 3
Summary of HQSAR analysis for the set of BE and accelerators used in the study.

PLS analysis	HQSAR
Components	1
q^2	0.733
Conventional r^2	0.99
Standard error of estimate	0.046
F values	63.243
Bootstrapping	
r^2	0.737
Standard error of estimate boot strapping	0.042
Progress scrambling	
Q^2	0.637
cSDEP	0.05
$dq^{2\prime}/dr^{2\prime}_{yy}$	1.7
Predictive r^2	0.718

Table 4
Predicted EC_{50} values for binder's effective (BE) and accelerators using HQSAR analysis.

Compound	Experimental EC_{50} (μM)	Predicted EC_{50} (μM)	residual
gfp66*	7.02	7.189	−0.156
gpf04	7.16	7.15	0.024
GFP33	7.17	7.18	0.003
GFP72	7.17	7.169	0.014
gfp75	7.17	7.164	0.019
GFP16	7.17	7.169	0.014
GJP58	7.18	7.18	0.013
gfp80*	7.18	7.277	-0.088
GJP43	7.19	7.193	0.009
GFP22	7.19	7.204	-0.002
GJP30	7.2	7.198	0.014
gfp88	7.23	7.232	0.011
GJP91	7.23	7.24	0.001
GJP50	7.24	7.244	0.007
GFP01*	7.24	7.313	-0.065
gjp51	7.24	7.231	0.020
gfp06	7.25	7.252	-0.008
GJP52	7.26	7.264	0.006
GJP32	7.27	7.261	0.010
GJP14	7.28	7.279	0.010
gjp36	7.29	7.289	0.01
GJP49	7.32	7.321	0.007
gjp45*	7.37	7.28	0.099
GFP07	7.42	7.418	-0.006
GFP23	7.43	7.43	0.004

2.5. Atomic contribution maps of the effective binder (GFP23) and accelerator (GFP22) using HQSAR

The HQSAR model is graphically represented in the form of contribution maps where the color of each atom reflects the contribution of that atom to the molecule's overall activity. The atoms with different color codes reflects the degree of contribution to the overall antiprion activity of the compound. The atoms with poor (or negative) contributions to the biological activity was shown with red end of the spectrum (red, red orange, and orange), while the atoms with favorable (positive) contributions was shown with green end (yellow, green blue, and blue). Atoms with intermediate contribution was shown in white color. Fig. 6A and B shows the individual atomic contribution to the EB (GFP23) and ACC (GFP22) to its antiprion activity.

The results indicate that the benzamide and 1H-indole groups mainly contributes the overall antiprion activity of the EB

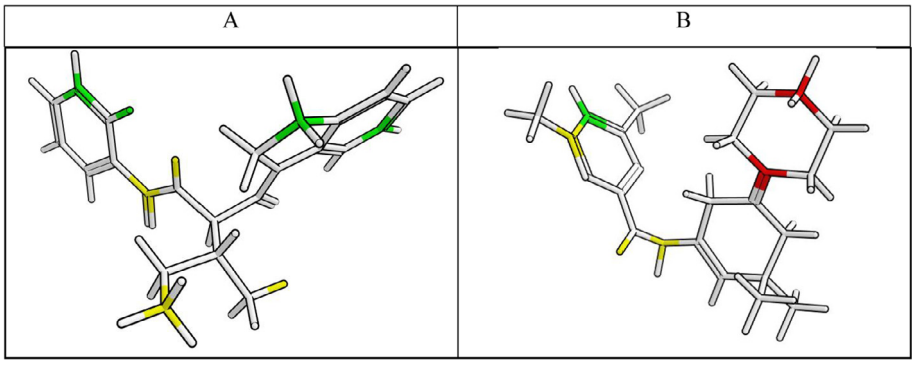

Fig. 6. HQSAR contribution maps of inhibitor (GFP23) (Fig. A) and accelerator (GFP22) (Fig. B) for prion protein $SHaPrP^{C}$ inhibition and acceleration.

Table 5
Dataset used for HQSAR study.

Comp	IUPAC name	Mean level of PrPSc ± SD (%)
GFP66*	2-(6,7-Dihydro-5*H*-cyclopenta[4,5]thieno[2,3-*d*]pyrimidin-4-ylsulfanyl)-*N*-(tetrahydrofuran-2-ylmethyl) acetamide	93.68 ± 13.69
GFP04	2-(6,7-Dihydro-5*H*-cyclopenta[4,5]thieno[2,3-*d*]pyrimidin-4-yloxy)-*N*-(2-methylcyclohexyl)acetamide	68.77 ± 11.7
GFP33	*N*-(3-Cyano-4,5,6,7-tetrahydro-1-benzothiophen-2-yl)-4,5,6,7-tetrahydro-1-benzothiophene-2-carboxamide	66.94 ± 0.11
GFP72	(4*R*)-1-[2-Oxo-2-(piperidin-1-yl)ethyl]-3′,4′-dihydro-2*H*,2′*H*,5*H*-spiro[imidazolidine-4,1′-naphthalene]-2,5-dione	67.11 ± 33.65
GFP75	1-(2-Methyl-2,3-dihydro-1*H*-indol-1-yl)-2-(thieno[2,3-*d*]pyrimidin-4-yloxy)ethanone	67.43 ± 23.22
GFP16	1-(3,4-Dihydroquinolin-1(2*H*)-yl)-2-[(2*R*)-2-propyl-2,3-dihydro-1*H*-benzimidazol-1-yl]ethanone	67.24 ± 1.24
GJP58	*N*-[(1*R*,2*R*,4*S*)-bicyclo[2.2.1]hept-2-yl]-2-(2-oxobenzo[*cd*]indol-1(2*H*)-yl)acetamide	65.03 ± 4.59
GFP80*	3-(4-Oxo-3,4-dihydroquinazolin-2-yl)-*N*-(1,2,3,4-tetrahydronaphthalen-1-yl)propanamide	65.01 ± 35.45
GJP43	N^2-Cyclopentyl-N^1-phenylpyrrolidine-1,2-dicarboxamide	63.16 ± 7.91
GJP22	1-(2,3-Dihydro-1*H*-indol-1-yl)-2-[(3*R*)-3,5,6,7-tetrahydro-2*H*-indeno[5,6-*b*]furan-3-yl] ethanone	63.70 ± 5.23
GJP30	2-(Cyclopentylamino)-2-oxoethyl 2,3-dihydro-1*H*-cyclopenta[*b*]quinoline-9-carboxylate	62.89 ± 3.93
GJP91	*N*-[(2*R*,3*S*,3a*R*,7a*S*)-3-Cyanooctahydro-1-benzothiophen-2-yl]-2-[(2*R*)-2-methylpiperidin-1-yl]acetamide	58.78 ± 5.89
GJP50	4-[2-(3,4-Dihydroquinolin-1(2*H*)-yl)-2-oxoethyl]-2*H*-1,4-benzoxazin-3(4*H*)-one	57.55 ± 4.88
GFP01*	*N*-(Ethenylcarbamoyl)-2-acetamide	56.73 ± 13.15
GJP51	(2*E*)-*N*-(Thiophen-2-yl)-2-(2,3,3-trimethyl-3,4-dihydroisoquinolin-1(2*H*)-ylidene)ethanamide	57.44 ± 1.62
GFP06	2-(2,3-Dihydro-1*H*-indol-3-yl)-*N*-(1,2,3,4-tetrahydronaphthalen-2-yl) acetamide	55.33 ± 12.35
GJP52		54.71 ± 9.21
GJP32	(1*R*)-1,4-Dihydronaphthalen-1-yloxo[(2*R*)-1,2,3,4-tetrahydronaphthalen-2-ylamino]acetate	53.05 ± 10.72
GJP14		51.32 ± 7.76
GJP36	2-[4-(Cyclobutylcarbonyl)-1,4-diazepan-1-yl]-8-methylquinoline-3-carbonitrile	50.62 ± 21.26
GJP49	8-Methyl-7-{[2-(piperidin-1-yl)ethyl]sulfanyl}-2,3-dihydro[1,4]dioxino[2,3-*g*]quinoline	47.40 ± 19.89
GJP45*	3-Amino-*N*-cyclopentyl-8-methylthieno[2,3-*b*]quinoline-2-carboxamide	41.85 ± 18.82
GFP07	2-[2-(Butylamino)-1*H*-benzimidazol-1-yl]-1-(2,3-dihydro-1*H*-indol-1-yl) ethanone	37.33 ± 4.23
GFP23	*N*-[1-(2,3-Dihydro-1*H*-indol-1-yl)-3-methyl-1-oxopentan-2-yl]benzamide	36.78 ± 0.63

representing with the green and yellow (Fig. 6A). These colors indicate positive contribution to the activity of the EB, suggesting that this is a pharmacologically important group for effective binders that inhibit $SHaPrP^{Sc}$ formation by stabilizing $SHaPrP^{C}$. The particular atoms of the EB with positive contributions to activity include, C1, C4, H4, C7, H7, C8, H8, C12, H12, H1, C20 and H21. The attachment of 5,5-dimethylcyclohex-3-en-1-ylidene}-1?5-piperidin-1-ylium to the backbone of 1-{3-[2-(4,6-dimethylpyrimidin-2-yl) hydrazin-1-yl] creates a negative contribution to the antiprion activity of ACC shown with red color (Fig. 6B). To verify predictability of the constructed HQSAR model based on the training set, four compounds were selected as testing set for validation. The predicted bioactivities of the training and test sets were shown in Table 5. The correlation between the predicted and experimental results was depicted in Fig. S3. The PLS analysis on the test set released cross validated q2 value of 0.73 and r2 value of 0.73 with a standard error of 0.046 (Table 4). In addition, the predictive r2 value of 0.73 may suggest a satisfactory model. All of the statistical results demonstrate that the HQSAR model is fairly reliable with good predictive ability and could be helpful in discovering new antiprion compounds. Superimposition of the EB and ACC compounds showed that biologically active groups of 1-oxopentan-2-yl]benzamide of EB and 1-{3-[2-(4,6-dimethylpyrimidin-2-yl) hydrazin-1-yl] of ACC align each other with an overall alignment score of -59 kcal/mol (Fig. 7).

2.6. Docking versus CoMFA of the EB (GFP23) and ACC (GFP22)

The CoMFA analysis of steric and electrostatic contour maps of the EB and ACC is shown in Fig. 8. These contour maps were compared and contrasted with the docking orientations in the binding site of $SHaPrP^{C}$. The green contours near the benzamide group of the EB (GFP23) fell in the hydrophobic pocket-D formed between α2 and α3, while the green counters near pyramidine-2 amine group of ACCs (GFP22) is solvent exposed. The aliphatic side chains of Phe^{198}, Ile^{184}, Ile^{205}, Val^{209}, and Val^{210} lining the hydrophobic pocket make contacts with benzamide group of the EB (GFP23) (Fig. 8A). This indicates that benzamide group of the EB (GFP23) is favorable for $SHaPrP^{C}$ inhibition and thus preventing the conversion from $SHaPrP^{C}$-$SHaPrP^{Sc}$ while 1-(3,3-dimethylcyclohexylidene)piperidinium of the ACC (GFP22) is favorable for prion misfolding accelerating the conversion of PrP^{C} to PrP^{Sc} (Fig. 8B). Thus, contour maps generated by CoMFA are in good agreement with our docking studies which indicates that the results are highly reliable.

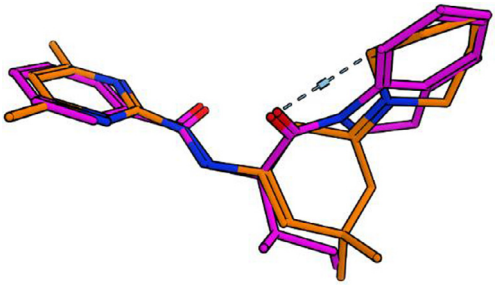

Fig. 7. Superimposition of Inhibitor (GFP23) and accelerator (GFP22) using MOE software suite. Inhibitor is represented in magenta while the accelerator is represented in orange color.

2.7. Scaffold docking and virtual screening

A total of 1000 compounds were generated by recap synthesis with a set of 10 identified EB's GFP04, GFP06, GFP23, GFP75, GFP80, GJP14, GJP45, GJP49, GJP51 and GJP52. These new compounds were again docked with $SHaPrP^{C}$ using the same method described above. The top-ranking molecule 4-[(7-amino-2,3-dihydro-1,3-benzothiazol-2-yl)oxy]-6,7-dimethoxy-2*H*-chromen-2-one had reasonable interactions and geometry fitting in the pocket-D of $SHaPrP^{C}$ (Fig. 9A). The O24 atom of the molecule showed hydrogen bonding interactions with O1 of Thr^{191}. Additionally, two hydrophobic interactions were observed between the carbon atoms, C10 and C11 of 6,7-diethyl-4-hydroxy-2*H*-chromen-2-one with Cβ of Phe^{198} and C of Met^{206}. The binding mode of this molecule shows that chromen-2-one group of the ligand orients deeper into the binding pocket and 2,3-dihydroxy-1,3-benzothiazol-7-amine group is on the surface region of the pocket-D. The benzothiazol group shows hydrogen- bonding interactions with the side chains of Arg^{156} (Fig. 9A). Finally, this molecule was used as a lead molecule for further virtual screening against the MOE database (Fig. 9B).

In total, 100 hit compounds were sorted out by applying a maximum fit value of 85 using 2D finger print analysis. In these set of 100 molecules, the scaffold molecule showed a very good similarity with six representative compounds that was chosen previously for fluorescence quenching studies against $SHaPrP^{C13}$ (Fig. S10). These six molecules were further used for densitometric analysis with a dose-dependent inhibition of $SHaPrP^{Sc}$ formation of ScN2a cells.

2.8. Comparison of ScN2a results with docking studies of six new inhibitors

The densitometric analysis of previously identified six antiprion compounds were carried out in a multi well format and PrP^{Sc} levels were measured by immunoblot of proteinase K-digested samples (Fig. 10).

Cells treated with DMSO (carrier) and quinacrine (a known antiprion drug) were used as negative and positive controls, respectively.[18] These measurements were used as reference to calculate the normalized percentage change in PrP^{Sc} levels following treatment of previously identified six compounds. Prion infected ScN2a cells were treated with these six compounds for 5 days at a concentration of 10, 20, 50 and 100 μM. Changes in PK-resistant PrP^{Sc} levels were analyzed by Western blots. We were able to confirm the antiprion activity of these six compounds in reducingPrP^{Sc} levels in ScN2a cells without being cytotoxic. Previous results of evaluation of the binding affinity between PrP^{C} and these six compounds using fluorescence quenching also confirmed that these

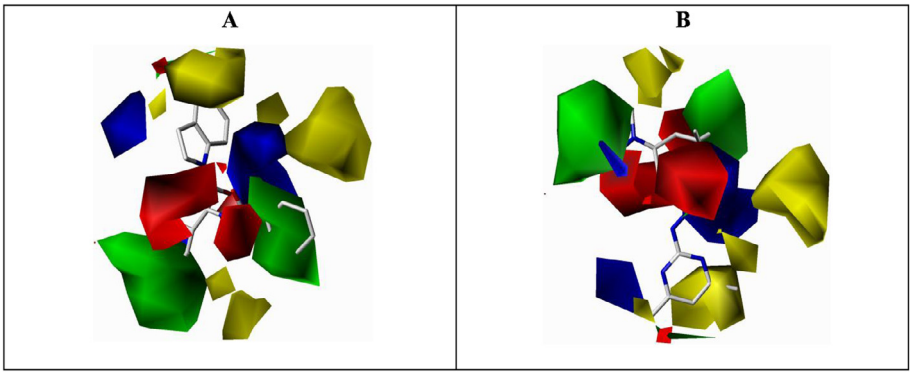

Fig. 8. CoMFA contribution maps of the inhibitor (GFP23) (Fig. A) and the accelerator (GFP22) (Fig. B) for prion protein inhibition and acceleration from $SHaPrP^{C}$-$SHaPrP^{Sc.}$

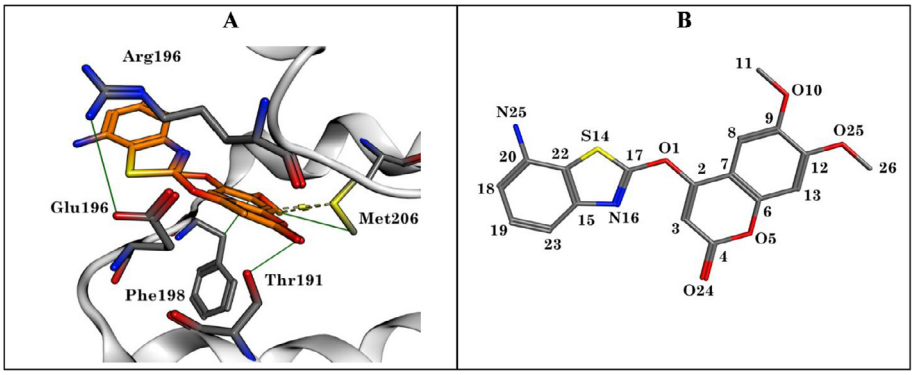

Fig. 9. Ligand protein interactions of molecular scaffold with pocket-D (Fig. A). The scaffold generated from a set of 10 identified inhibitors (Fig. B).

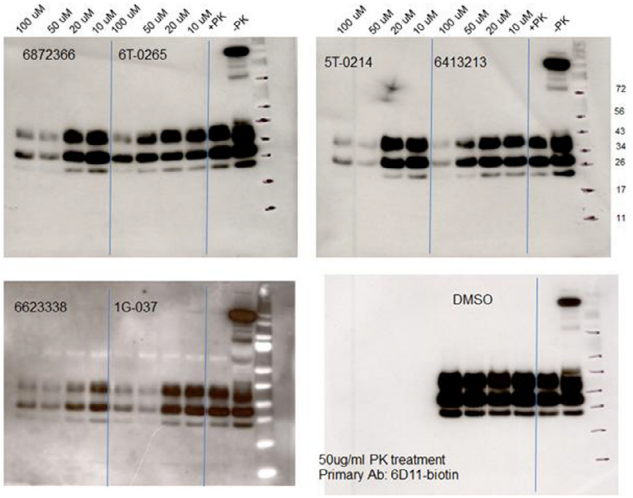

Fig. 10. Six representative compounds from MOE database that inhibit the PK^{res} PrP in ScN2a cells.

molecules bind to pocket-D of PrP^{C}.[13] This shows clearly that they may act by stabilizing PrP^{C}, thereby reducing the pool of substrate for conversion to PrP^{Sc}. The compound 3 (6T-0265) interacts with Arg^{156} and presents the poorest IC_{50} of the group showing greater than 100 μM. This is attributed to possible destabilization of the salt bridge that is formed with Glu^{196}. The compound 2 (5T-0214) contains a six-member ring that positions the nitrogen far enough away to avoid a water mediated hydrogen bond. Although, the compound does not penetrate deeper into the hydrophobic pocket, but still shows a better IC_{50} compared with compound 3 of ~35 μM. The other 2-amino pyrimidine compound1 (1G-037) orients opposite to compound 2 (5T-0214) and buries deeper into the pocket with a similar IC_{50} value of ~35 μM. The fused ring structure of compound 6 (6,623,338) works similar to GFP23, in that it appears to cover the pocket occupied by the *o,m*-methyl ether phenyl group with an IC_{50} of ~20 μM. While compound4 (6,413,213) buries much of the pockets surface area, with less hydrophobic interactions resulting in a weak K_d of 185 μM. Further

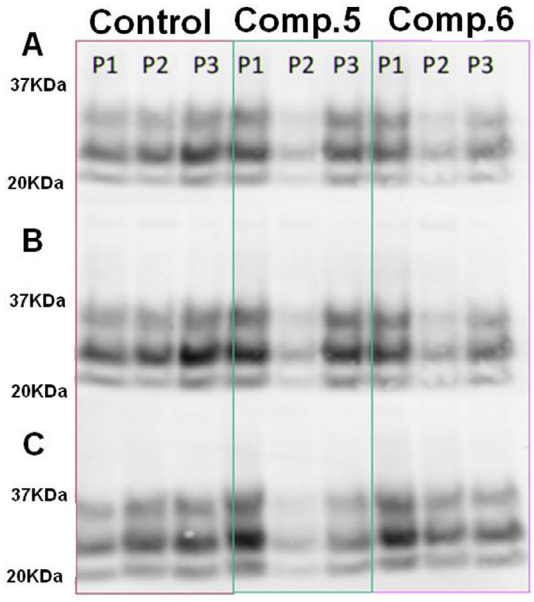

Fig. 11. Immunoblot for the compounds 5& 6 that inhibit PrP^{Sc} in ScN2a cells infected with RML strain.

disruption of R^{156}'s salt bridge is attributed to its poor IC_{50} value of ~75 μM. Lastly, the compound5 with smaller surface area (6,872,366) penetrates deep into the hydrophobic pocket and shows contacts with Arg^{156}'s side chain without disrupting the salt bridge with Glu^{196}. Thus, it displays a respectable IC_{50} of ~35 μM due to its binding pocket stabilization effects. Fluorescence quenching studies showed that compounds 3 and 6 binds with more stronger affinities with $SHaPrP^{C}$, with an estimated binding constant (K_d) of 15.5 and 46.4 μM compared to other 3 compounds studied.[13] This shows that compound3 although binds with higher affinity shows less inhibition constant compared to other compounds used for the study. Also, the study proves that compound6 is found to be very good inhibitor both in terms of binding and inhibition of scrapie form PrP^{Sc} in ScN2a cells. Furthermore, Immunoblots of PrP^{Sc} in ScN2a cells infected with RML strain showed reduction of prion infection signal in the second passage with compound5 and to some extent with compound6, but the signal returned in passage 3 (Fig. 11).

These results suggest that compounds 5 and 6 acts as promising leads in developing new antiprion compounds for prion disease therapy that potentially resists oligomerization.

2.9. Cytotoxicity assay in ScN2a cells infected with a rodent-adapted RML scrapie strain

Preliminary studies on cytotoxic effect of ScN2a cells as determined by MTS calorimetric solution showed no significant cell death in either #6 or #5 at 10, 30 and 100 μM for 21.5 h. Both compounds 6 and 5 didn't show significant toxicity at 10 and 30 μM. Moreover, Compound 5 showed no significant difference in cell viability even at 100 μM concentration.

2.10. Six representative antiprion compounds and EBs stabilizes the β2-α2 loop through allosteric interactions

The residues of pocket-A within the β2-α2 loop are within ~10 Å from the binding pocket-D where EBs and ACCs bind. Experimental evidence implicates this loop region in initiating PrP^{Sc} formation and possibly influencing inter species scrapie transmission.[19,20] Our previous fluorescence quenching studies also proves noscapine binding to pocket-A at the rigid loop and disturb the salt bridge between Arg^{164}/Asp^{178} initiating prion conversion from $SHaPrP^{C}$-$SHaPrP^{Sc}$. It was observed that the compounds EB (GFP23) (Fig. 12A), Bionet1G-037 (Fig. 12B), Bionet5T-0214 (Fig. 12C), Bionet6T-0265 (Fig. 12D), Chembridge6413213 (Fig. 12E), Chembridge6872366 (Fig. 12F), and Chembridge6623338 (Fig. 12G) binding to pocket-D influences the inward movement of the side chain, Tyr^{128} of β^{1} to orient ~59.6 ± 10° at Chi-2.

This inward shift of Tyr^{128} makes the aromatic side chain to move ~3.78Å closer toward Ile^{182} in α2 to form H—Pi interaction thereby increasing the hydrophobic contact surface. This orientation of the side chain appears to be an essential feature that could provide a stabilizing effect on the β1-β2 sheet as well as on the β2-α2 loop region. The cation-pi interaction is also observed between the side chains of Gln^{186}, Leu^{130} and Tyr^{162} that are separated by 4 Å apart (Fig. 4A). Additionally, in the bound state of the inhibitors, the hydrogen bonding interaction between Tyr^{128} and the backbone atom of Leu^{125} allows nitrogen atom of Arg^{164} to make a hydrogen bonding interaction with back bone of Gly^{127} (Fig. 4A). Additionally, hydrogen bonds are formed between Tyr^{163}-Cys^{179} and Tyr^{162}-Thr^{183} in the inhibitor bound conformations of Bionet1G-037, Chembridge-6413213, and Chembridge-6623338. This shows that the bound state of the β2-α2 loop appears to be more stable and is most likely preventing an easy transitioning of the Tyr^{169} side chain conformation. In the unbound $SHaPrP^{C}$ structure,

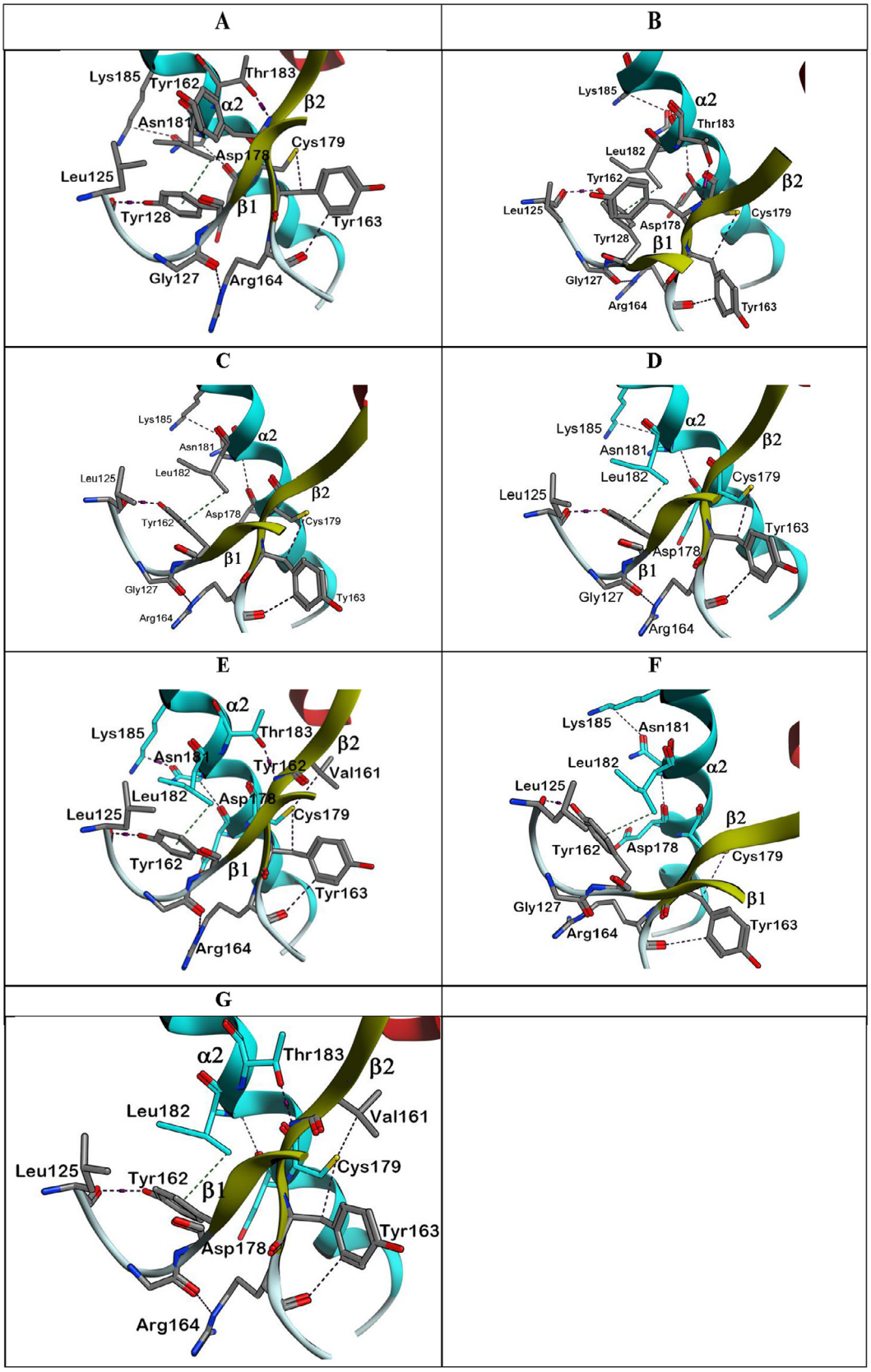

Fig. 12. Electrostatic interactions of Pocket-A of SHaPrP^{C} in the bound form of the inhibitors, GFP23 (Fig. A), Bionet1G-037 (Fig. B), Bionet5T-0214 (Fig. C), Bionet6T-0265 (Fig. D), Chembridge 6413213 (Fig. E), Chembridge 6872366 (Fig. F), Chembridge 6623338 (Fig. G).

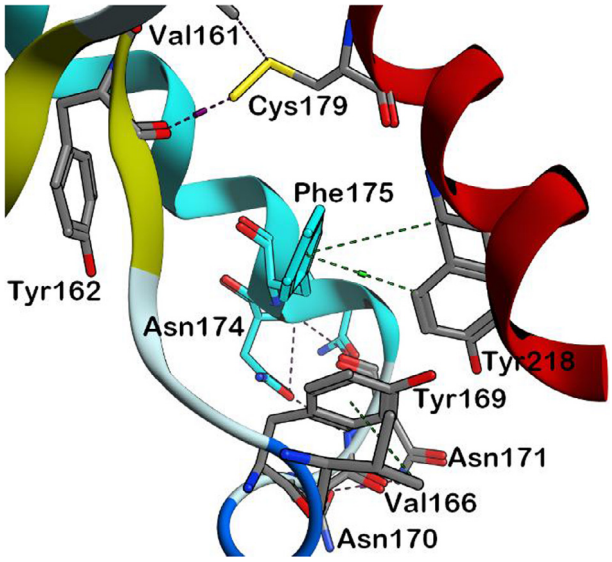

Fig. 13. Electrostatic interactions of Pocket-A of native form of SHaPrP$^{C.}$

no hydrogen bond is observed between β2-α2 loop conformations (Fig. 13).

However, Phe^{175} of α2 shows H—Pi interacts with Tyr^{128} of α3. This shows that the bound and free states exhibit completely different β2-α2 loop conformations. Furthermore, in the absence of the ligand, Tyr^{128} and Ile^{182} are separated by 5.11Å, disrupting the potentially stabilizing cation-pi interaction between these side chains (Fig. 4B). In addition, Tyr^{169} in the β2-α2 loop shows H—Pi interaction with Val^{166}, while Tyr^{162} shows hydrogen bonding with Cys^{179}. The relative positions of the polar residues Arg^{164}, Asp^{167}, and Gln^{168} in the β2-α2 loop also change depending on the loop backbone conformation.

2.11. Accelerators (ACCs) destabilizes the β2-α2 loop

Although binding of an ACC (GFP22) to pocket-D influences the inward movement of Tyr^{128} of β1 to form H—Pi interaction with

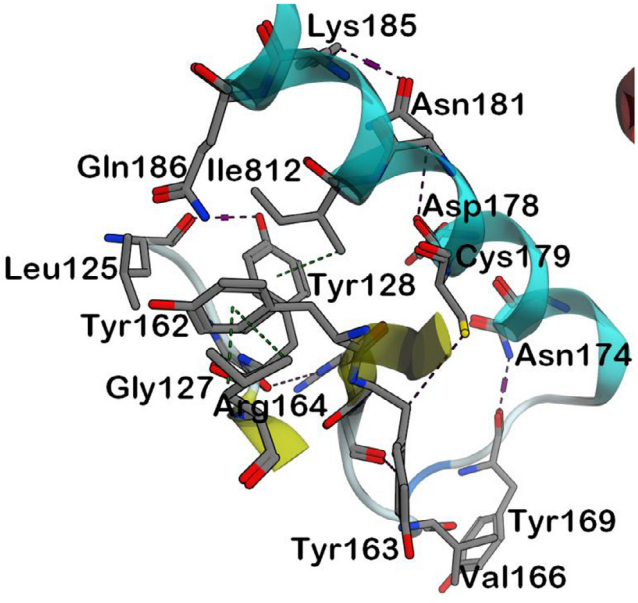

Fig. 14. Electrostatic interactions of Pocket-A of SHaPrP^{C} in the bound form of the accelerator (GFP22).

Ile^{182}, no cation-pi interactions were observed between the side chains of Gln^{186} and Tyr^{162} residues (Fig. 14). In addition, no H—Pi interaction was seen between Tyr^{169} of β2-α2 loop with Val^{166} even though Tyr^{163} shows hydrogen bonding with Cys^{179}. This orientation of Tyr^{169} and lack of H—Pi interactions between Gln^{186} and Tyr^{162} residues may destabilize β1-β2 sheet as well the β2-α2 loop region.

Overall, the docking studies clearly showed the difference in binding mode of EBs and six new antiprion compounds with that of ACCs, although all the three sets of molecules recognize the same binding pocket-D of SHaPrP^{C}. Structural superposition of the prion protein SHaPrP^{C} in the free (1B10.pdb) and ligand bound states of all the EBs, six new antiprion compounds and ACCs have an overall root-mean-square deviation (rmsd) of 0.3 Å for the Ca atoms (residues 125–225), indicating that there are no significant structural changes in the folded prion domain upon compound binding. However, the side chains of the residues involved in the interaction with EBs, six new antiprion compounds and ACCs showed conformational changes that accommodate the hydrophobic ligand inside the binding pocket-D. In the bound structure of the EB (GFP23), the side chain of Phe^{198} shifts by 108^{0} at the Cβ position, accommodating a hydrophobic contact with the benzamide group of the inhibitor ring. This contact may allow the side chain to hold the salt bridge Arg^{156}/Glu^{196}/Glu^{200} within the binding pocket intact. In the bound conformation of the ACC (GFP22), the C_{α} atom of residue Phe^{198} showed a shift of 4–5 Å that results in a movement of Arg^{156} away from Glu^{196}, rendering the binding pocket more accessible. This result may break the salt bridge between the residues Arg^{156}/Glu^{196}/Glu^{200} and allows the protein to misfolded. We speculate that the SHaPrP^{C} structure of bound ACCs may represent an inter-mediate stage encountered while making its passage through the binding pocket. The residues Met^{134} in loop1 between β1 and α1, Tyr^{149} in α1, Met^{154}, Arg^{156} and Tyr^{157} in loop 2 between α1 and α2, Ile^{184} in α2, Gly^{195}, Asn^{197} and Phe^{198} in loop3 between α2 and α3, and Ile^{205}, Met^{206}, Val^{209} and Val^{210} residues in α3 acts as common pharmacophores of these EBs and six new antiprion compounds preventing the SHaPrP^{C} conversion to pathogenic form SHaPrP^{Sc}.[13] Most of the residues displaying significant side chain orientation on binding to these EBs and six new antiprion compounds were found to cluster into two separate regions of the SHaPrP^{C}. The first region is the α2-α3 loop and the neighboring residues in helices α2 and α3. The second region is α1, specifically those residues in contact with α3. This show that these EBs and new antiprion compounds show specific interactions commonly at pocket-D of SHaPrP^{C} and may maintain the salt bridge between Arg^{156}/Glu^{196}/Asp^{202} intact for effective antiprion activity. Specifically, these compounds mainly to interact with Phe^{198} through hydrophobic contact and prevent its exposure between the oligomers to generate larger aggregates.[21] The contour maps of CoMFA generated from the 3D QSAR models built using pharmacophore based alignment highlight the interaction sites responsible for differences in the biological activity. Green indicates the contour regions where the bulky substituent would increase the inhibitory activity, while the yellow outline indicates the regions where steric bulk would be unfavorable to the inhibitory activity of SHaPrP^{C}. CoMFA contour maps of the steric and electrostatic properties of the EB (GFP23) gives the highest affinity with the series (0.11 mM) as shown in Fig. 8A. The large green contour found around the benzamide group of the EB (GFP23) indicates that a bulky group of this position provides support for the high antiprion activity. However, the green counter is far from 1-(3,3-dimethylcyclohexylidene)piperidinium ring of the ACC (GFP22) towards solvent exposed. This is perhaps why the EB (GFP23) with benzamide group that occupy the green counter in the buried region acts as an inhibitor than the compound with pyramidine-2 amine that acts as an accelerator. The presence

of yellow contours near the 1H indole group of the EB indicates it is unfavorable for the antiprion activity. Moreover, the unfavorable yellow contour was observed near the di-methylcyclohexylidene piperidinium ring of the accelerator. This indicates that di-methylcyclohexylidene piperidinium ring would significantly reduce the aggregation of PrP^{Sc} with a mean level of 63.70 ± 5.23. The CoMFA electrostatic contour mapped marked by red and blue contours, including red regions show areas where more negatively charged groups are favorable to inhibitory activity and blue colored regions represent areas where increased positively charged groups are favorable to antiprion activity. The red contour map near an oxymethyl group indicates that electronegative group is favored at the *meta* position of the phenyl ring. The phenyl and 1H indole portion of the EB (GFP23) 1-(3,3-dimethylcyclohexylidene)piperidinium ring and pyramidine-2 amine of the ACC (GFP22) are occupied by large blue contours due to the presence of the electron-withdrawing nitrogen atoms. The large blue contour shows that an electron-deficient nature is important for high binding affinity. The electronegative carbonyl oxygen atom of the oxymethyl group forms a favorable contact with the positively charged nitrogen atom of Asn^{197} surrounded by a blue contour. The electrostatic interactions with these backbone atoms are essential for differentiation in potency of the EB (GFP23) and ACC (GFP22). The red contours with the high electron density of the EB (GFP23) are in close proximity to the electronegative group of Met^{206}-SCH3 justifying the presence of red and yellow contours. However, the red contours with the high electron density of the ACC are solvent exposed without showing any contact indicating the role in prion misfolding. Our NMR chemical shift data also indicate that EB (GFP23) binding perturbs the interface between helices α2-α3, supporting the idea that EB (GFP23) binding may allosterically enhanced the packing between the helices. This flexible prion region, the C-terminal part of helix α2 and the α2-α3 loop, is the recognition site for antiprion compound GN8, a small molecule that prolongs the survival of TSE-infected mice.[8] The results also showed that residues such as Phe^{198} in the α2-α3 loop, and Val^{203}, Met^{206}, and Val^{210} in α3 also show chemical shifts changes for the backbone amides along with Thr^{188} within α2. As a result, the relative orientation between α1 and α3 is $\sim -70°$.[22] This orientation further stabilizes the salt bridge between Arg^{156}/Glu^{196} using α2-α3 loop only in $SHaPrP^{C}$ (1uw3). These strong interactions are not found in either huPrP, in which this region is involved in the hinge of the swapped dimer, or antibody-bound $SHaPrP^{C}$, being this region the antibody epitope. These specific interactions may also be advantageous to reducing side effects. Previous ^{1H}–^{15N} HSQC spectra of PrP^{C} with or without GJP49 shows the specific binding of GJP49 to the C-terminal region of α2 and at part of the α2-α3 loop of PrP^{C} with a dissociation constant (K_d) of 50.8 μM.[15] Further, six active antiprion compounds that were previously identified were tested by a high-throughput, ELISA-based assay utilizing ScN2a cells. Reductions in the expression level of $SHaPrP^{C}$ by two new antiprion compounds at 20 (compound 6) and 32 μM (compound 5) concentration represent a promising mechanism of action for prion pathogenic inhibition from PrP^{C}-PrP^{Sc}. The compounds 6 and 5 have not shown any sign of toxicity in a standard MTS assay at 30 μM concentration. However, compound6 with high antiprion activity with IC_{50} of 20 μM compared to compound5 raises the possibility that compound6 might serve as a lead compound for prion therapy. These results and previous fluorescence quenching studies suggest that all of these six new antiprion compounds directly interacted with recombinant $SHaPrP^{C}$ in GN8 binding site. Although the mechanisms of action of these compounds are unclear in vitro, fluorescence quenching analysis suggests that they are likely to interact directly with $SHaPrP^{C}$ at pocket-D and may stabilize the slat bridge between Arg^{156}/Glu^{196}/Glu^{200}. Thus, these six new antiprion compounds can be referred to as "medical chaperones" that stabilized the native conformation of the target protein $SHaPrP^{C}$ and inhibit its transition to the abnormal conformation, $SHaPrP^{Sc}$. Thus, based on the present and previous studies, it can be stated that compound6 stabilizes $SHaPrP^{C}$ specifically more than any other compound used in the study and could be used as a therapeutic candidate for prion diseases.

3. Conclusions

In this study, we have successfully combined the docking, HQSAR, CoMFA, NMR and cell based assays to observe the binding effect of EB (GFP23), ACC (GFP22) on prion stabilization and misfolding. The good correlation obtained between the molecular docking and experimental studies show that the EBs, ACCs bind to pocket-D of $SHaPrP^{C}$. In addition, the docking results also show that the EBs maintain the salt bridge between Arg^{156}-Glu^{196} while ACCs disturb the salt bridge. In addition, virtual screening of the compounds database using the molecular scaffold identified six compounds in the ranking list of 100 that were previously identified as antiprion compounds. The compounds 6 & 1, 2 & 5 with an estimated IC_{50} value of 20 μM and ~35 μM shows significant effect in reducing accumulation of $SHaPrP^{Sc}$ in ScN2a cells in the micromolar range. These were non-toxic to cultured cells with good bioavailability consistent with central nervous system. Fluorescence quenching and computational studies conducted previously on these six compounds showed that compound6 bind to pocket-D of $SHaPrP^{C}$ with a K_d value of 44 μM and in addition may effectively maintains the salt bridge between Arg^{156}/Glu^{196}/Glu^{200}. In combination, our results also indicate that newly screened compound6 is more potent than other compounds in stabilize $SHaPrP^{C}$ in preventing its conversion into $SHaPrP^{Sc}$. Thus, this study will be useful for the designing more novel compounds using compound6 for prion protein inhibition from PrP^{C} to PrP^{Sc}. These results also indicate that our computational studies show very good correlation with experimental studies.

4. Methodology

4.1. Molecular docking

For *In silico* docking in MOE (Chemical computing group, Montreal, Canada), the ligand placement method "Alpha PMI" was employed using London dG scoring function using implicit generalized born solvation model.[23] The simulated annealing based on the Monte Carlo method was used to find the global minimum of the ligand. It explores various states of a configuration space by generating small random changes in the current state and then accepts or rejects each new state according to the Metropolis criterion.[24] The ligand was optimized by energy minimization with the Tripos Assisted Force Field (TAFF) until the energy gradient is below 0.001 kcal/Mol.[25] By default, thirty conformations docked as a cut-off were retained. Finally, affinity scoring function, ΔG (Utotal in kcal/mol), was employed to rank a candidate poses as the sum of the electrostatic and Van der Waals energies. This method may generate bound conformations that resemble resolutions close to crystallography.[26] The dielectric function based on the reaction model with a cut-off between 8 and 10 Å was used for our docking studies with the pocket radius of 6. The pharmacophoric model that was generated using recap synthesis and binds with higher affinity in pocket-D was used as a scaffold for virtual screening. The compounds with maximum fit value of 85 were chosen for ScN2a cell based assay to determine the IC_{50} values against the conversion of PrP^{C} to PrP^{Sc}.

4.2. NMR studies

NMR spectra were acquired at 25 °C on a 500 MHz Varian Unity INOVA spectrometer fitted with a 5 mm HCN z-gradient pulsed-field gradient cryogenic probe except for the STD-TOCSY, which was collected at 25 °C on an 800 MHz Varian Unity INOVA spectrometer fitted with a 5 mm HCN xyz-gradient pulsed-field gradient cryogenic probe. All experiments were collected using Varian BioPack pulse sequences (VNMRJ v2.1B). Spectra were processed using nmrpipe and analyzed with nmrpipe and nmrviewj unless stated otherwise.[27] Both inhibitor (GFP23) and accelerator (GFP22) used in the study was purchased from Sigma-Aldrich (St. Louis, MI, USA), and used without further purification. To collect the first NOESY NMR spectrum, each compound was dissolved in 20 mm potassium phosphate buffer at pH 6.5 giving a final concentration of 100 lm. Ten percent (v/v) D_2O was added to each sample to maintain a spectral lock, 1 mm of 2,2-dimethyl-2-silapentane-5-sulfonate was added for chemical shift referencing.[28] For each 1D NOESY spectrum, 48,000 points were averaged from 256 transients over a sweep width of 6000 Hz. A recycle delay of 0.01 s and an acquisition time of 4 s were used. The mixing time for the screening experiments was 100 ms. Immediately following collection of the reference compound spectra, the NMR sample was used to reconstitute prealiquoted, lyophilized $SHaPrP^C$ (90–232) and a second spectrum was collected with the same parameters. The molar ratio of protein to each compound was 1:1. Matching spectra were superposed and analyzed with the Chenomx NMR suite v6.0 to assess chemical shift and linewidth perturbations of the metabolite signals. To collect the 2D 15N-HSQC titration spectra, a reference 15N-HSQC spectrum of the $SHaPrP^C$ (90–232), alone, was first collected (300 lm, 350 lL, 20 mm KH2PO4, pH 7 and 6.2). These 15N-HSQC reference spectra were collected with 2048 complex points in the 1H dimension and 256 complex points in the 15N dimension using a recycle delay of 1.5 s (nt = 120, sw = 6000 Hz, sw1 = 1800 Hz). Each compound was successively added to concentrations of 1, 2, 5 and 10 mm and the 15N-HSQC spectra recollected using identical acquisition parameters. The amide chemical shift data for the EB (GFP23) and ACC (GFP22) complex has been deposited into the {[1-(2-methylpropyl)-1*H*-benzimidazol-2-yl] sulfanyl}BioMagResBank (BMR17834).

4.3. HQSAR and CoMFA analysis of EB (GFP23) and ACC (GFP22)

The series of antiprion compounds used for the HQSAR and CoMFA analysis include EBs and ACC derivatives were obtained from a report published by Hosokawa-muto et al.[8] The report consists of 27 compounds with mean level of PrP^{Sc} using two to four independent experiments (Table 5).

The compound structures were built in SybylX2.0 molecular modeling package and Gasteiger–Marshili charges were assigned to the atoms of the compounds. All the compounds were energy minimized until the gradient convergence of 0.001 $kcal^{-1}\ A^{-1}$ was reached using Tripos force field (http://www.tripos.com/). The compounds in the dataset were divided into training and test set. From these 25 compounds, only 21 compounds were selected as training set and four compounds (1, 9, 16 and 24) were taken as a test set. The mean values of the training set were converted into their logarithmic form (−log50) and subsequently used as dependent variables in the HQSAR analysis. The compounds in the training set were used to derive the model whereas; the compounds in the test set were used to evaluate the predictability of the model.

4.4. 2D fingerprint based similarity search

The 2D similarity searches were performed with the software MOE [Molecular Operating Environment Montreal, Quebec, Canada: Chemical Computing Group, Inc.; 2007] using two-point (typed graph distances (TGD) and three-point (typed graph triangles (TGT) pharmacophore-based fingerprints, all calculated from a 2D molecular graph. Each atom was given a type among donor, acceptor, polar, anion, cation, or hydrophobe for the calculation of TGD and TGT. Subsequently, pairs (two-point fingerprint) or triplets (three-point fingerprints) of types were formed by graph distances and coded as sparse features in a fingerprint. The Tanimoto coefficient was used as the similarity metric.[29] The Tanimoto coefficient between two molecules described by a 2D fingerprint is calculated using the following expression:

$$T_{ab} = C/a + b - c$$

where "c" is the number of bits common to the two molecules, and "a" and "b" denote the number of bits set in each of the two fingerprints.

4.5. ScN2a cell line assay-1

The chemical library of six compounds that were used for screening in cell-based assays was commercially obtained from BioNet and Chembridge databases.[13] Compounds were solubilized at 10 mm in dimethyl sulfoxide (DMSO)[2] and stored in a 96-well format. Furthermore, a mouse neuroblastoma (N2a) cell line was infected with the Rocky Mountain Laboratory (RML) strain of scrapie prions to produce ScN2a cells.[30] Screening the chemical library for antiprion activity was performed in a high-throughput ELISA. Briefly, 4 × 104 ScN2a cells were treated with these six compounds of interest for 21.5 h at 10, 20, 50 and 100 μM concentrations. ScN2a cells treated with quinacrine (1 μm) were used as positive controls while cells treated with DMSO alone was used as Negative controls.[18,31] Cells were lysed with lysis buffer (0.5% Nonidet P-40, 0.5% deoxycholate, 10 mm Tris-HCl, pH 8, 100 mm NaCl) and protein concentration was normalized to 1 mg/ml using the BCA assay. Samples were incubated with 20 μg/ml of proteinase K for 1 h at 37 °C. Digestions were stopped with 2 mm phenylmethylsulfonyl fluoride (PMSF), and samples were centrifuged at 100,000×*g* for 1 h at 4 °C. Supernatants were discarded, and pellets were re-suspended in reducing SDS sample buffer for SDS-PAGE. After treatment and cell lysis, normalized crude extracts were analyzed by Western immunoblotting using conjugated 6D11-biotin antibody to detect PrP. For dose–response analysis, ScN2a cells were treated for 21.5 h at 10, 20, 50 and 100 μM and quantified by Western immunoblotting as described above.

4.6. ScN2a cell line assay-2

Mouse neuroblastoma cell lines (N2a) infected with a rodent-adapted RML scrapie strain were treated with prion conversion inhibitors and were tested for ongoing infection by immunoblot assay of protease resistant prion protein (PrP^{Sc}) in cell lysates. Cell cultures were treated with individual therapeutic compounds including compounds 5 & 6 with fresh drug present in the media with each passage and cell collection every 2–3 days. Samples were taken though multiple passages to allow clearance of infection and monitoring for any adaptation resulting in re-emergence of a drug-resistant or drug-dependent strain of PrP^{res}.

4.7. Cytotoxicity assay in ScN2a cells infected with a rodent-adapted RML scrapie strain

For preliminary toxicity experiments, cultures were plated onto 96-well plates in triplicates for 21.5 h at different concentrations of compound6 (3 μM, 10 μM, 30 μM) and compound 5 (10 μM, 30 μM

and 100 μM). Cytotoxicity was evaluated by the 3-[(4,5-dimethylthiazol-2-yl)-5,3-carboxymethoxyphenyl]-2-(4-sulfophenyl)-2*H* tetrazolium, inner salt (MTS) reduction assay (Promega). Cells were incubated with MTS solution (2 mg/mL) for 2 h at 37 °C in a 5% CO_2 incubator, then read at 490 nm using a Spectramax M5 spectrophotometer. P values lower than 0.05 were considered significant. Cell viability was calculated as percent of control, with control being non-treated cells.

A. Supplementary data

Supplementary data associated with this article can be found, in the online version, at http://dx.doi.org/10.1016/j.bmc.2017.09.024.

References

1. Prusiner SB. Novel proteinaceous infectious particles cause scrapie. *Science*. 1982;216:136–144.
2. Prusiner SB. Prions. *Proc Natl Acad Sci USA*. 1998;95:13363–13383.
3. Kocisko DA, Baron GS, Rubenstein R, Chen J, Kuizon S, Caughey B. New inhibitors of scrapie-associated prion protein formation in a library of 2000 drugs and natural products. *J Virol*. 2003;77:10288–10294.
4. Guest WC, Cashman NR, Plotkin SS. Electrostatics in the stability and misfolding of the prion protein: salt bridges, self energy, and solvation. *Biochem Cell Biol*. 2010;88:371–381.
5. Trevitt CR, Collinge J. A systematic review of prion therapeutics in experimental models. *Brain*. 2006;129:2241–2265.
6. Kimata A, Nakagawa H, Ohyama R, et al. New series of antiprion compounds: pyrazolone derivatives have the potent activity of inhibiting protease-resistant prion protein accumulation. *J Med Chem*. 2007;50:5053–5056.
7. Caughey B, Caughey WS, Kocisko DA, Lee KS, Silveira JR, Morrey JD. Prions and transmissible spongiform encephalopathy (TSE) chemotherapeutics: A common mechanism for anti-TSE compounds? *Acc Chem Res*. 2006;39:646–653.
8. Kuwata K, Nishida N, Matsumoto T, et al. Hot spots in prion protein for pathogenic conversion. *Proc Natl Acad Sci USA*. 2007;104:11921–11926.
9. Gallardo-Godoy A, Gever J, Fife KL, Silber BM, Prusiner SB, Renslo AR. 2-Aminothiazoles as therapeutic leads for prion diseases. *J Med Chem*. 2011;54:1010–1021.
10. Hosokawa-Muto J, Kamatari YO, Nakamura HK, Kuwata K. Variety of antiprion compounds discovered through an in silico screen based on cellular-form prion protein structure: Correlation between antiprion activity and binding affinity. *Antimicrob Agents Chemother*. 2009;53:765–771.
11. Silber BM, Gever JR, Li Z, et al. Antiprion compounds that reduce PrP(Sc) levels in dividing and stationary-phase cells. *Bioorg Med Chem*. 2013;21:7999–8012.
12. Cramer RD, Patterson DE, Bunce JD. Comparative molecular field analysis (CoMFA). 1. Effect of shape on binding of steroids to carrier proteins. *J Am Chem Soc*. 1988;110:5959–5967.
13. Pagadala NS, Perez-Pineiro R, Wishart DS, Tuszynski JA. In silico studies and fluorescence binding assays of potential anti-prion compounds reveal an important binding site for prion inhibition from PrP(C) to PrP(Sc). *Eur J Med Chem*. 2015;91:118–131.
14. Kimura T, Hosokawa-Muto J, Asami K, Murai T, Kuwata K. Synthesis of 9-substituted 2,3,4,9-tetrahydro-1H-carbazole derivatives and evaluation of their anti-prion activity in TSE-infected cells. *Eur J Med Chem*. 2011;46:5675–5679.
15. Kuwata K, Kamatari YO, Akasaka K, James TL. Slow conformational dynamics in the hamster prion protein. *Biochemistry*. 2004;43:4439–4446.
16. Pagadala NS, Bjorndahl TC, Blinov N, Kovalenko A, Wishart DS. Molecular docking of thiamine reveals similarity in binding properties between the prion protein and other thiamine-binding proteins. *J Mol Model*. 2013;19:5225–5235.
17. Christen B, Hornemann S, Damberger FF, Wuthrich K. Prion protein NMR structure from tammar wallaby (Macropus eugenii) shows that the beta2-alpha2 loop is modulated by long-range sequence effects. *J Mol Biol*. 2009;389:833–845.
18. Korth C, May BC, Cohen FE, Prusiner SB. Acridine and phenothiazine derivatives as pharmacotherapeutics for prion disease. *Proc Natl Acad Sci USA*. 2001;98:9836–9841.
19. Damberger FF, Christen B, Perez DR, Hornemann S, Wuthrich K. Cellular prion protein conformation and function. *Proc Natl Acad Sci USA*. 2011;108:17308–17313.
20. Sigurdson CJ, Joshi-Barr S, Bett C, et al. Spongiform encephalopathy in transgenic mice expressing a point mutation in the beta2-alpha2 loop of the prion protein. *J Neurosci*. 2011;31:13840–13847.
21. Chen W, van der Kamp MW, Daggett V. Structural and dynamic properties of the human prion protein. *Biophys J*. 2014;106:1152–1163.
22. Pastore A, Zagari A. A structural overview of the vertebrate prion proteins. *Prion.*. 2007;1:185–197.
23. Mackerell Jr AD, Feig M, Brooks 3rd CL. Extending the treatment of backbone energetics in protein force fields: limitations of gas-phase quantum mechanics in reproducing protein conformational distributions in molecular dynamics simulations. *J Comput Chem*. 2004;25:1400–1415.
24. Metropolis N, Ulam S. The Monte Carlo method. *J Am Stat Assoc*. 1949;44:335–341.
25. Krebs-Smith SM, Clark LD. Validation of a nutrient adequacy score for use with women and children. *J Am Diet Assoc*. 1989;89:775–783.
26. Goto J, Kataoka R, Hirayama N. Ph4Dock: pharmacophore-based protein-ligand docking. *J Med Chem*. 2004;47:6804–6811.
27. Delaglio F, Grzesiek S, Vuister GW, Zhu G, Pfeifer J, Bax A. NMRPipe: a multidimensional spectral processing system based on UNIX pipes. *J Biomol NMR*. 1995;6:277–293.
28. Wishart DS, Bigam CG, Yao J, et al. 1H, 13C and 15N chemical shift referencing in biomolecular NMR. *J Biomol NMR*. 1995;6:135–140.
29. Rogers DJ, Tanimoto TT. A computer program for classifying plants. *Science*. 1960;132:1115–1118.
30. Bosque PJ, Prusiner SB. Cultured cell sublines highly susceptible to prion infection. *J Virol*. 2000;74:4377–4386.
31. May BC, Fafarman AT, Hong SB, et al. Potent inhibition of scrapie prion replication in cultured cells by bis-acridines. *Proc Natl Acad Sci USA*. 2003;100:3416–3421.